Lattice location of the group V elements Sb, As, and P in ZnO

Ulrich Wahl *[a,b], João Guilherme Correia [a,b,c], Tânia Mendonça [d], Stefan Decoster[e]
[a] Instituto Tecnológico e Nuclear, Estrada Nacional 10, 2686-953 Sacavém, Portugal
[b]Centro de Física Nuclear da Universidade de Lisboa, Av. Prof. Gama Pinto 2, 1649-003 Lisboa, Portugal
[c]CERN-PH, 1211 Genève 23, Switzerland
[d]Departamento da Física, Universidade do Porto, Rua do Campo Alegre 687, 4169-007 Porto, Portugal
[e]Instituut voor Kern- en Stralingsfysica and INPAC, Katholieke Universiteit Leuven, Celestijnenlaan 200D, 3001 Leuven, Belgium

ABSTRACT

Modifying the properties of ZnO by means of incorporating antimony, arsenic or phosphorus impurities is of interest since these group V elements have been reported in the literature among the few successful *p*-type dopants in this technologically promising II-VI compound. The lattice location of ion-implanted Sb, As, and P in ZnO single crystals was investigated by means of the electron emission channeling technique using the radioactive isotopes ^{124}Sb, ^{73}As and ^{33}P and it is found that they preferentially occupy substitutional Zn sites while the possible fractions on substitutional O sites are a few percent at maximum. The lattice site preference is understandable from the relatively large ionic size of the heavy mass group V elements. Unfortunately the presented results cannot finally settle the interesting issue whether substitutional Sb, As or P on oxygen sites or $Sb_{Zn}–2V_{Zn}$, $As_{Zn}–2V_{Zn}$ or $P_{Zn}–2V_{Zn}$ complexes (as suggested in the literature) are responsible for the acceptor action. However, the fact that the implanted group V ions prefer the substitutional Zn sites is clearly a strong argument in favour of the complex acceptor model, while it discourages the notion that Sb, As and P act as simple "chemical" acceptors in ZnO.

Keywords: zinc oxide, antimony, arsenic, phosphorus, lattice location, emission channeling

1. INTRODUCTION

To date, reproducible and controllable *p*-type doping and its theoretical understanding remains one of the key issues in the quest to realize optical and electrical devices based on the technologically promising II-VI compound ZnO. The group V elements nitrogen, phosphorus, arsenic and antimony have all been claimed in the literature as *p*-type dopants (for recent reviews on this subject see Ref. [1-5]). Even the heavy group V metal bismuth was reported to show acceptor action, although no *p*-type conduction could be achieved[6]. However, particularly in the cases of the heavy-mass group V dopants P, As, and Sb, which are in the focus of this paper, the exact mechanism of their acceptor action is still heavily debated, as will be discussed below.

Arsenic[7] and phosphorus[8] were the first heavy-mass group V elements for which *p*-type doping of ZnO was reported in 2000. In the meantime, As-doped *p*-type ZnO has been produced by means of pulsed laser deposition[7,9-12], hybrid beam deposition[13,14], evaporation and sputtering[15], ion implantation[16,17], radiofrequency (RF) magnetron sputtering[18], and metal-organic chemical vapor deposition (MOCVD)[19], and devices include ultraviolet (UV)[14,17] and visual-infrared light emitting diodes (LEDs)[19]. Succesful doping methods for P include excimer laser processing[8], diffusion[20,21], RF sputter deposition[22-26], molecular beam epitaxy (MBE)[27], MOCVD[28], and laser ablation[29]. However, so far mostly rectifying diodes have been demonstrated from *p*-ZnO:P[8,21,24,25] and only weak electroluminescence in the visible[8].

*uwahl@itn.pt; phone +351-219946085; fax +351-219946285; www.itn.pt

CERN-OPEN-2014-002
23/01/2010

Sb as *p*-type dopant in ZnO has recently attracted considerable attention due to the wide range of optoelectronic devices that have been fabricated using MBE[30-35] or MOCVD[36] grown layers. While the first report[37] of Sb-doped *p*-type ZnO using excimer laser processing dates back to 2002, the introduction of MBE growth for Sb doping followed later[38-40], pursued by pulsed laser deposition[41] and thermal oxidation[42]. The impressive list of devices based on *p*-ZnO:Sb layers now includes homo- and heterojunction photodiodes[30,31], UV LEDs[32-34,36], and UV lasers[35].

While there is little doubt that the relatively small N^{3-} ion (ionic radius 1.46 Å) replaces an O^{2-} anion (1.38 Å) in ZnO, acting as a singly ionized acceptor, the large size mismatch between O^{2-} and the potential acceptor ions P^{3-} (2.12 Å), As^{3-} (2.22 Å) or Sb^{3-} (2.45 Å) makes the simple substitution of O^{2-} anions unlikely[1,3]. On the other hand, the much smaller radii of the triply positive ions P^{3+} (0.44 Å), As^{3+} (0.58 Å) or Sb^{3+} (0.76 Å) should favour the substitution of Zn^{2+} (0.60 Å) cations, resulting in donor formation. With respect to ionic size, another possibility seems to be the replacement of O^{2-} by neutral As^0 or Sb^0, but this configuration would probably form a double donor. The radii of the corresponding ions in various configurations are illustrated in Fig. 1. Reaching beyond simple arguments of size, stability, chemical properties and oxidation state, density functional theory (DFT) indeed suggests that P_O, As_O or Sb_O (i.e. replacing oxygen) act as deep centers and not as shallow acceptors[43,44]. Also based on DFT results, the experimentally observed *p*-type behaviour was attributed to the formation of electrically active acceptor complexes of the type $P_{Zn}–2V_{Zn}$, $As_{Zn}–2V_{Zn}$ or $Sb_{Zn}–2V_{Zn}$, first predicted by Limpijumnong et al[44-47] for As and Sb and later by Shen et al[12] for P, the "complex acceptor model". While this concept is finding more and more acceptance[6,16,18,25,28,32,36,38-42], it is strongly disputed by others who support the point of view that P, As or Sb in ZnO act as simple chemical acceptors that replace oxygen[10,11,26,29,48], the "chemical acceptor model".

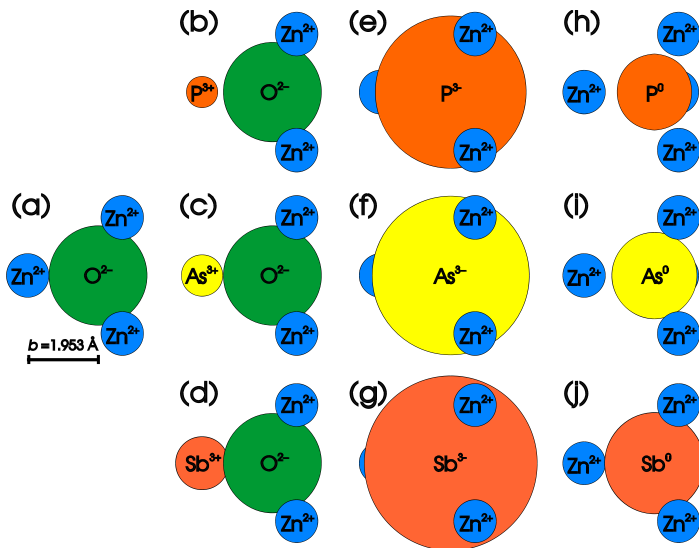

Figure 1. Ball model plots illustrating the ionic sizes of Zn, O, P, As, and Sb in zinc oxide. (a): In the undisturbed ZnO lattice, the bond length b = 1.953 Å between neighboring Zn and O atoms almost exactly matches the sum of the ionic radii of Zn^{2+} (0.60 Å) and O^{2-} (1.38 Å), illustrating the comparatively strong ionic character of the bonds. Note that the structure has been rotated in such a way that the straight line connecting the central O^{2-} ion with the leftmost Zn^{2+} ion lies within the horizontal plane. (b), (c), (d): The leftmost Zn^{2+} ion has been replaced with P^{3+}, As^{3+}, and Sb^{3+} ions of radius 0.44 Å, 0.58 Å, 0.74 Å, respectively, illustrating the relatively good size match between the triply positive group V ions and Zn^{2+}. (e), (f), (g): P^{3-}, As^{3-}, and Sb^{3-} ions with their large radii of 2.12 Å , 2.22 Å and 2.45 Å do not fit within the cage of the surrounding four Zn^{2+} ions. (h), (i), (j): In contrast, neutral P^0, As^0 or Sb^0 atoms with their covalent radii of 1.06 Å, 1.20 Å, and 1.40 Å would fit within the cage of the surrounding four Zn^{2+} ions.

In order to understand the mechanism of *p*-type doping in ZnO, experiments that reveal the lattice location of group V impurities are crucial. We have previously determined the lattice sites of ion implanted As and Sb in ZnO by means of

electron emission channeling from radioactive ^{73}As[49-52] and ^{124}Sb[52-53]. In this contribution we review these results and present also new data on emission channeling experiments using the implanted radioactive isotope ^{33}P.

2. EXPERIMENTAL

The emission channeling method[54] uses radioactive probe atoms that have been implanted into a single crystal sample. It is based on the fact that charged particles from nuclear decay (in our case conversion electrons or β^- particles) experience channeling or blocking effects along major crystallographic axes and planes. The resulting anisotropic emission yield from the crystal surface in the vicinity of axial and planar directions depends in a characteristic way on the lattice site(s) occupied by the probe atoms during decay. A typical emission channeling experiment is schematically illustrated in Fig. 2.

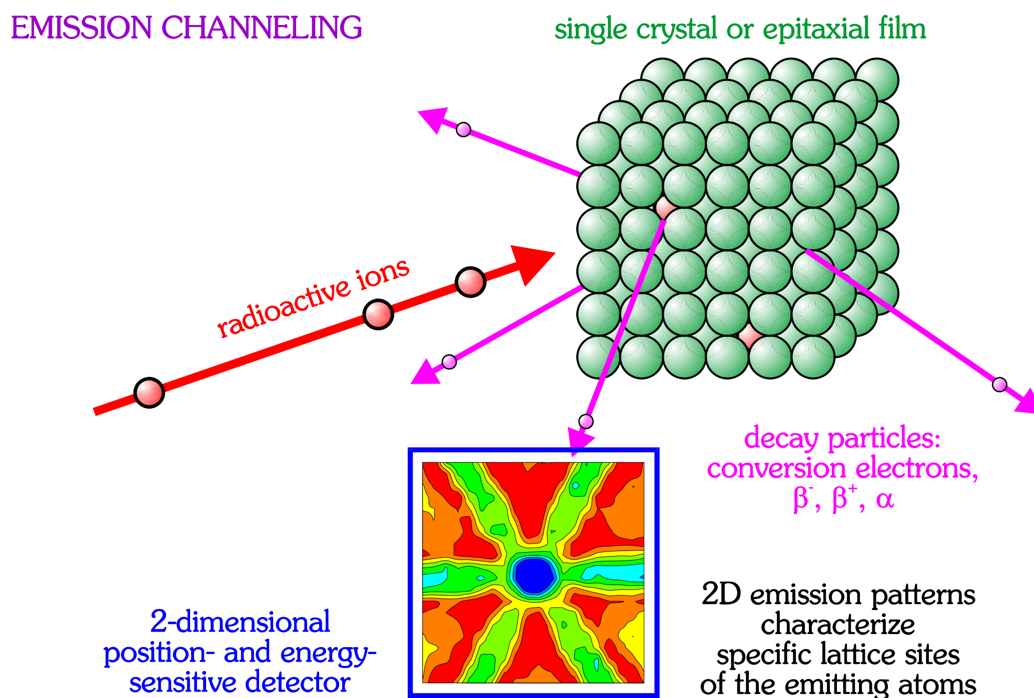

Figure 2. Illustration of a typical emission channeling experiment using radioactive probe atoms implanted into a single crystalline sample. Note that the size of the single crystal is of course greatly exaggerated in comparison to the detector. Also, many atomic layers underneath the surface contribute to the channeling effect.

For the experiments described below, *c*-axis oriented ZnO single crystals were implanted at room temperature with ^{73}As ($t_{1/2}$= 80.3 d), ^{124}Sb (60.2 d) and ^{33}P (25.3 d). While the sample implanted with ^{124}Sb was a hydrothermally grown, Zn-face oriented crystal obtained from CrysTec GmbH, the samples used for the ^{73}As and ^{33}P implantations were SCVT-grown, O-face oriented crystals purchased from Eagle Picher Technologies. The production and implantation of ^{73}As and ^{124}Sb were performed at CERN's on-line isotope separator facility ISOLDE, where beams of radioactive Sb ions are produced by nuclear reactions of a 1 GeV proton beam with UC_2 targets followed by resonant laser ionization[55], while radioactive As is obtained using ZrO_2 or Nb irradiation targets coupled to hot plasma ion sources. Since ISOLDE cannot produce phosphorus beams the isotope ^{33}P was commercially obtained as a solution of phosphoric acid and implanted using the ion implanter of IKS Leuven. The chosen implantation conditions were a fluence of 2×10^{13} cm^{-2} with 60 keV energy for ^{73}As, 1×10^{14} cm^{-2} with 30 keV for ^{124}Sb, and 1×10^{15} cm^{-2} with 60 keV for the ^{33}P implantation, all under angles of 7–10° with respect to the surface normal and collimated into a spot of 1 mm diameter. However, as was

obvious from the detected count rate during the emission channeling experiment, the $^{33}P^+$ implantation had suffered from an unknown contamination with the same charge over mass ratio, so that only around 0.5% of the implanted fluence was due to radioactive ^{33}P. Possible candidates for the contamination are the decay product of ^{33}P, i.e. stable ^{33}S, or $(^{16}O^{17}O)^+$ molecular ions. The depth profile corresponding to the implantation conditions described above is in the case of ^{73}As centered at a depth of 232 Å, with a straggling of 100 Å and an As peak concentration of $[As]_{max} \approx 8\times10^{18}$ atoms cm^{-3} or ≈ 190 ppm with respect to [Zn]. The corresponding numbers for ^{124}Sb are 119(45) Å, $[Sb]_{max} \approx 9\times10^{19}$ atoms cm^{-3} ≈ 0.2%. For the ^{33}P implantation the profile is 468(220) Å with $[P]_{max} \approx 9\times10^{17}$ atoms cm^{-3} ≈ 20 ppm, however, with a roughly 200 times higher concentration of the unknown contaminant.

The angular distributions of the emitted 42 keV and 52 keV conversion electrons resulting from the decay of ^{73}As and of β^- particles from the decay of ^{124}Sb (endpoint energy E_{max} = 2.30 MeV, average energy $\langle E \rangle$ =378 keV) and ^{33}P (E_{max} = 249 keV, $\langle E \rangle$ =77 keV) were recorded around the [0001], [−1102], [−1101] and [−2113] directions by means of a 3×3 cm^2 sized 22×22 pixel position- and energy-sensitive Si pad detector[56,57] at a distance of 30 cm from the sample. The angular resolution due to the size of the implanted spot on the sample and the position resolution of the detector was ~0.16° (standard deviation). The measurements were all carried out at room temperature and taken in the as-implanted state and following various 10 min annealing steps *in situ* under vacuum (< 10^{-5} mbar).

The evaluation of the probe atom lattice location was performed by quantitatively comparing the experimental angular-dependent count rate with theoretical patterns for different lattice sites, using the two-dimensional fit procedure described previously[56] and briefly outlined in the following. For each considered lattice site, the simulations result in two-dimensional patterns of electron emission probability, $\chi_{theo}(\theta,\phi)$, where θ and ϕ denote polar and azimuthal angles from the channeling axis. These patterns are smoothed using a Gaussian of $\sigma = 0.06°$ to account for that part of the experimental angular resolution which is due to the 1 mm beam spot on the sample. The size and shape of the detector pads, however, is taken into account during fitting by averaging over the simulated yield falling within the angular range (0.26°×0.26°) of one pad. Theoretical emission patterns are fitted to the experimental yields, χ_{ex}, according to

$$\chi_{ex}(\theta,\phi) = S\,[f_1\,\chi_{theo,1}(\theta,\phi) + f_2\,\chi_{theo,2}(\theta,\phi) + f_3\,\chi_{theo,3}(\theta,\phi) + 1 - f_1 - f_2 - f_3]$$

where S is a scaling factor common to all angles in one pattern, and f_1, f_2 and f_3 denote the fractions of emitter atoms on up to three different lattice sites. The random fraction, $f_R = 1-(f_1+f_2+f_3)$, accounts for emitter atoms which cause negligible anisotropies in emission yield, i.e. which are located in sites of very low crystal symmetry or in heavily damaged or amorphous surroundings. Thus up to seven fit parameters, S, f_1, f_2, f_3, x_0, y_0 and ϕ_0, may be simultaneously optimized using non-linear least square fitting routines. Note that the parameters S, x_0, y_0 and ϕ_0 are always needed in order to provide correct normalization of the experimental spectra and to achieve optimum translational and azimuthal orientation of the calculated patterns with respect to the measured ones.

In the fit procedure, we considered theoretical patterns resulting from emitter atoms at substitutional Zn (S_{Zn}) and O sites (S_O) with varying root mean square (rms) displacements, the main interstitial sites (Fig. 3) and a diversity of interstitial sites resulting from displacements along or off the *c*-axis[49]. The theoretical emission channeling patterns were calculated by means of the "manybeam" theory of electron diffraction in single-crystals[54]. The continuous electron spectrum from the β^- decay was approximated in the calculations by a histogram with stepwidths of 25 keV electron energy up to 800 keV, of 50 keV up to 1.4 MeV, and of 100 keV up to 2.3 MeV. The number of beams used was 16 up to 725 keV electron energy, 20 up to 950 keV and 24 at all higher energies. In order to describe the crystal structure of ZnO, we adopted the following model: lattice constants of a = 3.250 Å and c = 5.207 Å[58], together with a Zn-O *c*-axis bond length of $u = 0.375\,c$, as in an ideal wurtzite structure, and anisotropic rms displacements of $u_{\|}$(Zn) = 0.078 Å, $u_{\|}$(O) = 0.081 Å, $u_{\perp}$(Zn) = 0.090 Å and $u_{\perp}$(O) = 0.092 Å[59], where $u_{\|}$ and $u_{\perp}$ represent one-dimensionally projected rms displacements u_1 parallel and perpendicular to the c axis, respectively. Note that slightly higher values of the bond length parameter u than 0.375 may be found in the literature, e.g. 0.3825[59] and 0.3819[60], and also the reported values for the room temperature rms displacements[59-61] vary in the range u_1(Zn) = 0.078–0.097 Å and u_1(O) = 0.075–0.092 Å, however, it has been shown previously[62,63] that the outcome of the manybeam simulations is not overly sensitive to small variations in the bond length parameter parameter u or the rms displacements u_1.

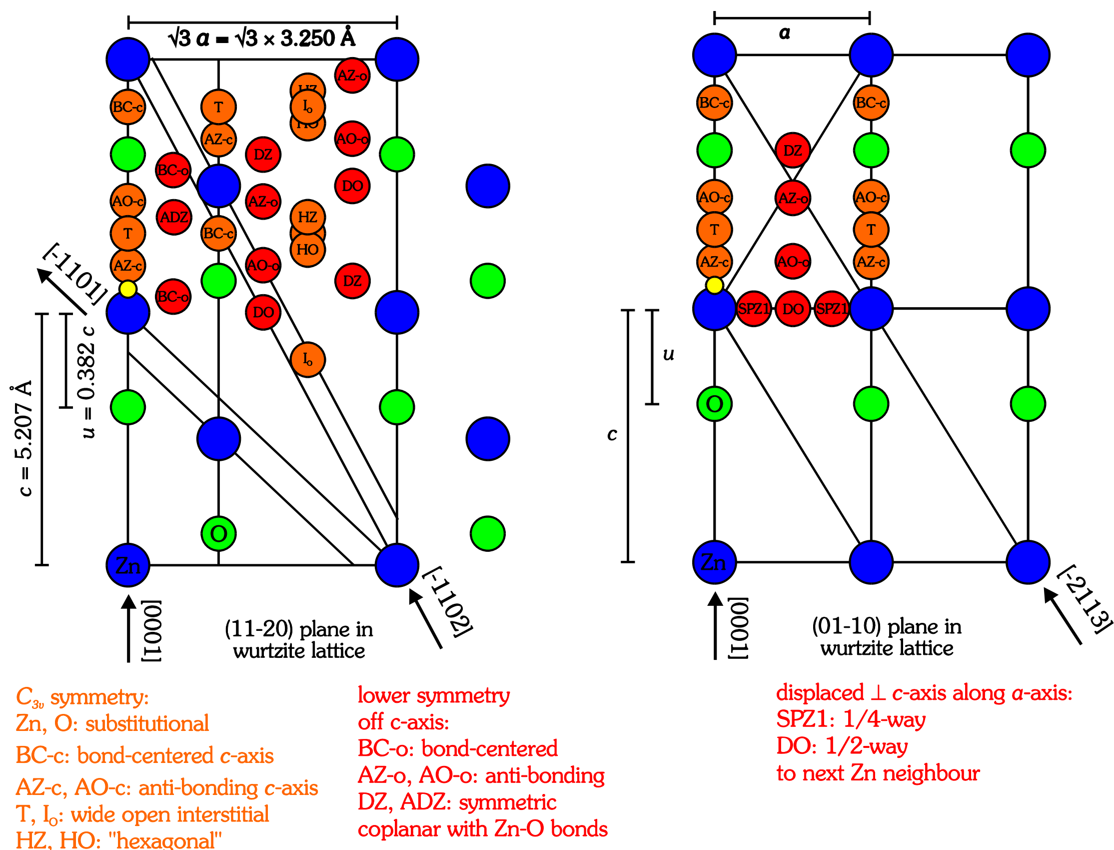

Figure 3. The (11–20) (left hand side) and (01–10) (right hand side) planes in the ZnO wurtzite lattice, showing the location of substitutional Zn sites, substitutional O sites, bond center BC, antibonding Zn (AZ) and antibonding O (AO), interstitial "octahedral" (I_O), "tetrahedral" (T) and "hexagonal" (HZ and HO). "-c" denotes sites within and "-o" off the *c*-axis. DZ and ADZ are interstitial sites which are coplanar with the Zn-O bonds, while SPZ1 and DO are sites which are displaced from Zn sites perpendicular to the *c*-axis along the *a*-axis. The filled yellow circles mark the approximate position of As within electrically active As_{Zn}–$2V_{Zn}$ complexes predicted by Ref. 44, for which calculated emission channeling effects are shown in Fig. 6 (m)-(p).

Since electrons have high cross sections for scattering, electron emission channeling experiments always require a correction for electrons which are backscattered from the sample and the walls of the vacuum setup into the detector. For conversion electron emitters such as ^{73}As the amount of elastically backscattered electrons can be corrected quite accurately by extrapolating the amount of inelastically scattered electrons at lower energies into a trapezoidal background that is subtracted from the conversion electron lines. In the case of ^{73}As, this method was used and resulted in the subtraction of a background of 39%. For β^- emitters such a procedure is not possible due to the continuous nature of the β^- spectra. The background contribution was estimated in this case by means of Monte-Carlo simulations based on the GEANT4 code[64], assuming isotropic electron emission from the radioactive source with energy distributions resulting from the β^- spectra of ^{124}Sb and ^{33}P and taking into account the elemental composition and geometrical features of the sample, the sample holder, and the vacuum setup. The experimental ^{124}Sb and ^{33}P patterns were thus corrected by subtracting isotropic background contributions in the detector of 49% and 27%, respectively.

3. RESULTS

3.1 Lattice location of implanted ^{73}As

Figure 4 (a-d) shows typical angular distribution patterns of conversion electrons within ±2.4° of four of the major crystallographic directions of the ^{73}As implanted ZnO sample. While the patterns were measured following 300°C annealing they are quite similar to those obtained in the as-implanted state (shown in Ref. [50]) or after 600°C annealing (shown in Ref. [51]). The channeling effect along the [0001] direction [Fig. 4 (a)] indicates that the majority of the ^{73}As probe atoms are located within the *c*-axis atomic rows. Fitting this experimental pattern by allowing only for probe atoms with positions centered within the *c*-axis rows and on random sites, resulted in the theoretical pattern shown in Fig. 4 (e), which corresponds to 94% of ^{73}As probe atoms along the *c*-axis with an rms displacement of $u_1(^{73}\mathrm{As}) = 0.13$ Å perpendicular to this direction.

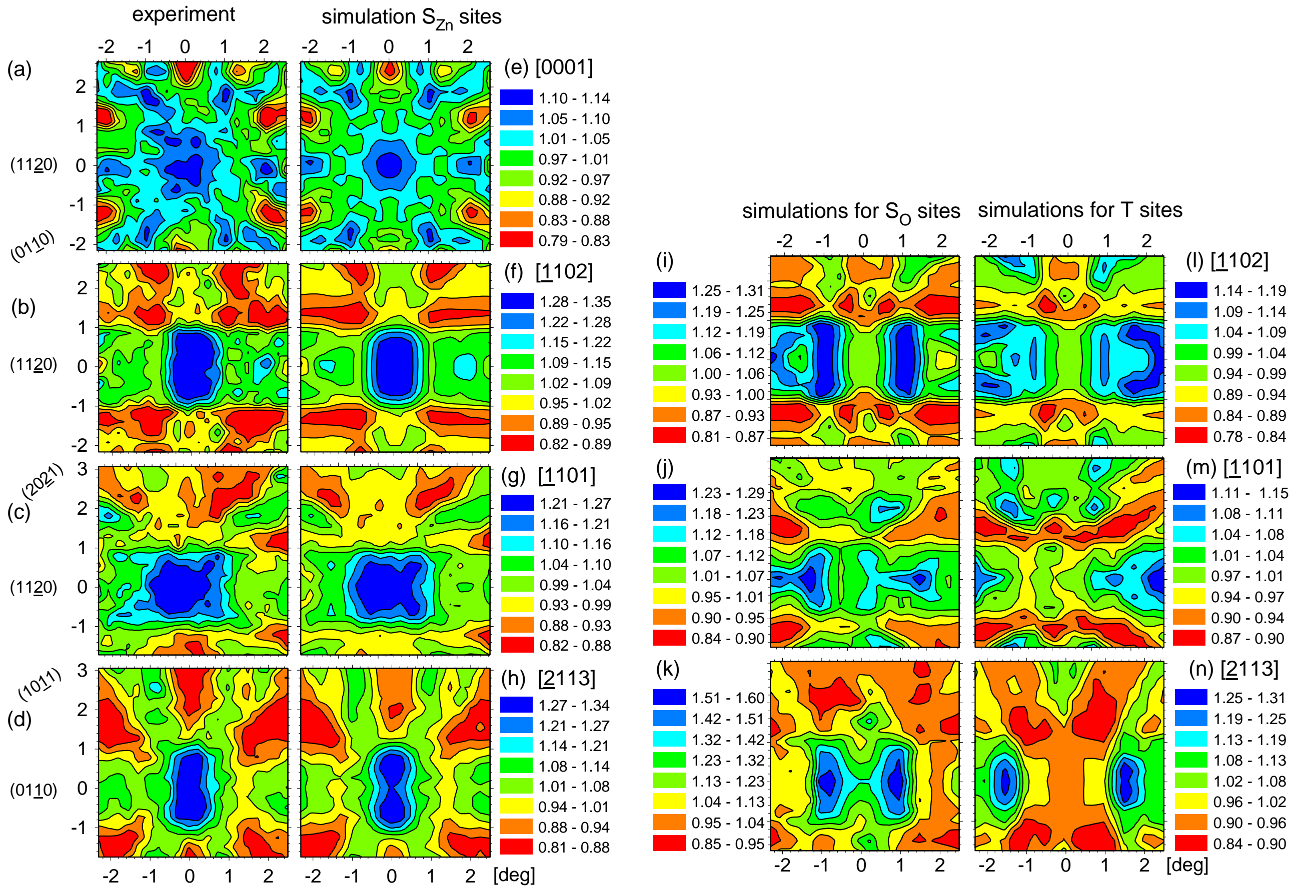

Figure 4. Normalized angular distribution of conversion electrons from ^{73}As→^{73}Ge in ZnO following 300°C annealing around the [0001] (a), [−1102] (b), [−1101] (c) and [−2113] (d) axis. (e)-(h): best fits of the channeling patterns for each direction, corresponding to 94% of probe atoms aligned with the *c*-axis and 83%, 98% and 91% at S_{Zn} sites. (i)-(k): Theoretical emission channeling patterns for 100% of emitter atoms on S_O sites. (l)-(n): Theoretical emission channeling patterns for 100% of ^{73}As on T sites. Note that the [0001] patterns for S_O and T sites are not shown since they are identical to the pattern for S_{Zn} sites.

It should be pointed out that c-axis patterns do not allow distinguishing between emitter atoms on S_{Zn} and S_O sites since both are aligned with the [0001] axis, along with a number of interstitial sites, e.g. the T sites (cf. Fig. 3). However, the site preference of As becomes clear when the [−1102], [−1101] and [−2113] experimental patterns are fitted in a similar way but allowing for emitter atoms on substitutional Zn and random sites. The resulting best fit theoretical patterns are

shown in Fig. 4 (f)-(h) and correspond to 83%, 98% and 91% at substitutional S_{Zn} sites with perpendicular ^{73}As rms displacements of 0.11 Å, 0.13 Å, and 0.11 Å, respectively. Major fractions of emitter atoms on other high-symmetric lattice sites than S_{Zn} can be ruled out. The theoretical channeling patterns from emitter atoms on substitutional O sites and interstitial T sites are shown for comparison in Fig. 4 (i)-(n). They are clearly incompatible with the experimental patterns.

In contrast to the experimental channeling patterns found in the as-implanted state and following 300°C and 600°C vacuum annealing, which could be very well fitted assuming only As on substitutional Zn sites and on random sites, following 900°C vacuum annealing an additional lattice site had to be introduced in the fits. Whereas the [0001] patterns remained relatively unaltered, showing that the probe atoms were still well-aligned with the *c*-axis, satisfactory fit results for the off-surface directions [−1102], [−1101] and [−2113] could only be obtained when also ^{73}As atoms located within 0.4 Å from tetrahedral interstitial T sites were allowed in the fits [Wahl 2005]. Note that the T sites are the major interstitial sites in the wurtzite structure that are aligned with the c-axis, making their [0001] emission channeling pattern identical to those of S_{Zn} and S_O sites.

In order to assess the possible fractions of ^{73}As emitter atoms on substitutional S_O sites and interstitial T sites, three-site fits were carried out, where, apart from random sites, fractions of emitter atoms on S_{Zn}, S_O and T sites were simultaneously allowed in the fits. The results as a function of annealing temperature are shown below in Fig. 8 (a). Already in the as-implanted state 73% of emitter atoms were found on S_{Zn} sites and we have indications that part of the rest is located on interstitial sites out of the *c*-axis, but we were not able to identify which interstitial site it might be. Upon annealing at 300°C the fraction on substitutional Zn sites reached a maximum around 90%, decreasing somewhat following the 600°C anneal, while after 900°C annealing ~30% occupied the interstitial T sites. Note that the fitted fractions on S_O or T sites are smaller than 5%, which is within the error bars of the accuracy of the method and hence not considered significant proof that these sites are actually occupied. The rms displacements from the ideal Zn positions were in all cases around 0.07–0.17 Å, i.e. somewhat larger than the thermal vibration amplitude of the Zn atoms [Fig. 8(d)].

3.2 Lattice location of implanted ^{124}Sb

Figure 5 (a)-(d) shows the angular-dependent emission yield of β^- particles from ^{124}Sb measured following annealing at 200°C around the four crystallographic directions of ZnO mentioned above. The fact that prominent channeling effects are observed for all four axial directions and for the major planes can only be explained by a large fraction of emitter atoms on substitutional sites. Note that the emission channeling effects due to the β^- particles from ^{124}Sb are considerably narrower than in the case of the conversion electrons from ^{73}As→^{73}Ge. This is due to the fact that the angular width of channeling effects decreases with increasing particle energy E roughly proportional $E^{-1/2}$. The best fits of theoretical patterns to the experimental data that allow for a fraction of emitter atoms on only one highly symmetric lattice site with the remainder on random sites, are shown in Fig. 5 (e)-(h). They were obtained for 65% of ^{124}Sb aligned with the *c*-axis, and 53%, 56% and 55% at substitutional S_{Zn} sites. The root mean square (rms) displacements perpendicular to the corresponding channeling directions, $u_1(^{124}\text{Sb})$, which gave the best fits were 0.11 Å, 0.12 Å, 0.17 Å, and 0.17 Å. As has been pointed out above already, emission channeling patterns resulting from emitter atoms on other lattice sites are distinctively different from the S_{Zn} site patterns and patterns calculated for ^{124}Sb emitter atoms on S_O sites are shown in Fig. 5 (i)-(l). Calculated patterns for a number of interstitial sites are shown: for T sites in Fig. 5 (m)-(p), for I_O sites in Fig. 6 (a)-(d), for DO sites sites in Fig. 6 (e)-(h), for ADZ sites sites in Fig. 6 (a)-(l), for S→AZ-c 0.5 sites (halfway between S_{Zn} and AZ-c) in Fig. 6 (m)-(p). Note that halfway between S_{Zn} and AZ-c (indicated by filled yellow circles in Fig. 3) is the approximate position of As within electrically active $As_{Zn}–2V_{Zn}$ complexes predicted by Ref. 44, which would probably be similar in the case of Sb. The experimental results are clearly not compatible with the majority of ^{124}Sb occupying any of these sites.

Figure 8 (b) below shows the fitted fractions of Sb emitter atoms as a function of annealing temperature when S_{Zn} as well as S_O and interstitial T sites were allowed in the fit. The fitted fractions for Sb on S_O or T sites are never larger than 5-6%, which is at the detection limit of the technique for this isotope (note that around half of the count rate resulted from scattered electrons). On the other hand, the fitted fraction of Sb on Zn sites is around 50-60% for annealing temperatures up to 600°C and then drops to 20% following 900°C vacuum annealing. The derived values for the rms displacements of ^{124}Sb [Fig. 8 (e)] are generally somewhat larger but close to those for Zn atoms at room temperature.

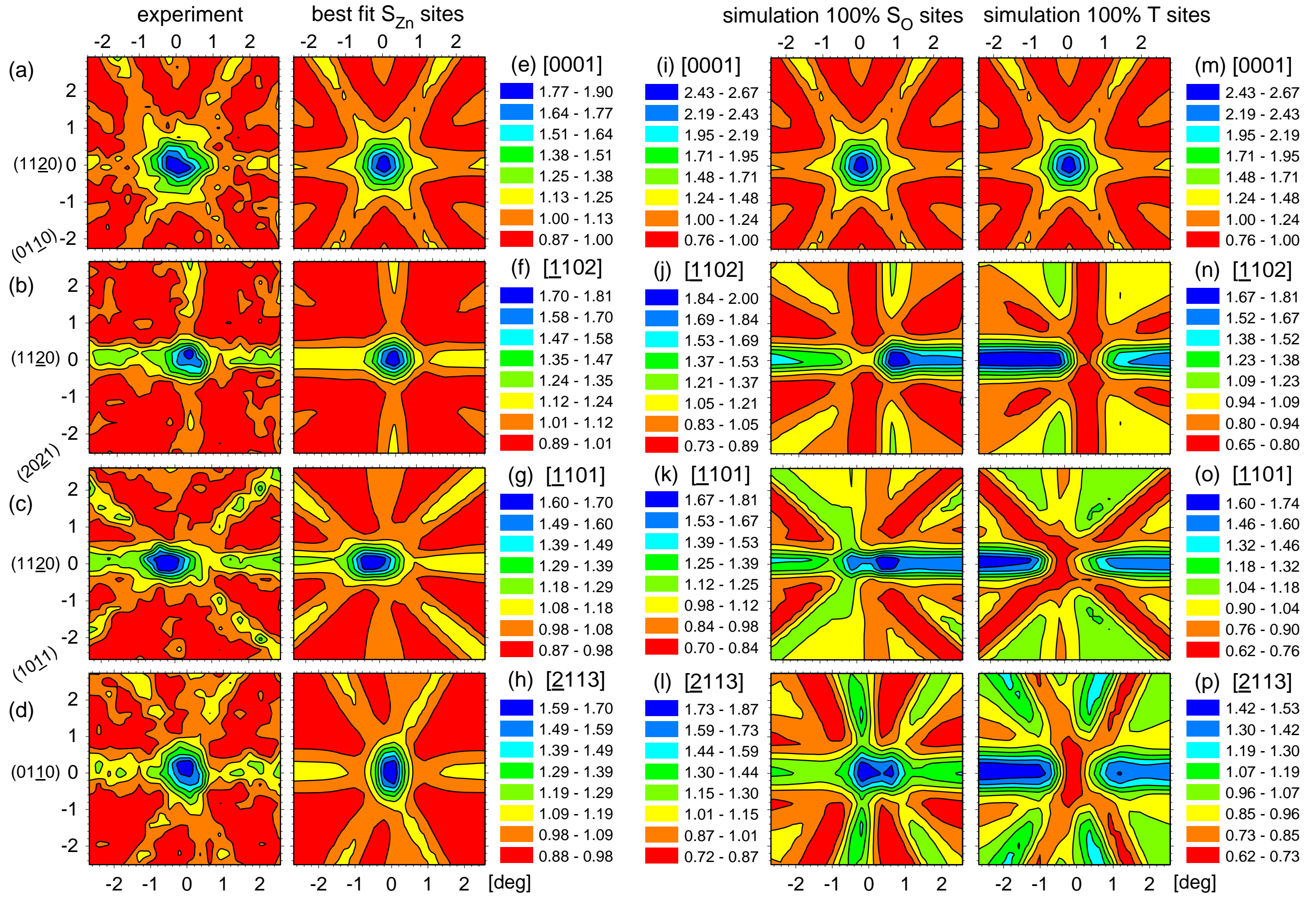

Figure 5. Normalized angular distribution of β^- yields from ^{124}Sb in ZnO following annealing at 200°C around the (a) [0001], (b) [−1102], (c) [−1101] and (d) [−2113] axis. (e)-(h): Best fits of the channeling patterns corresponding to 65% of ^{124}Sb aligned with the c-axis, and 53%, 56% and 55% at substitutional S_{Zn} sites, respectively. (i)-(l): Theoretical emission channeling patterns for 100% of emitter atoms on S_O sites. (m)-(p): Theoretical emission channeling patterns for 100% of ^{124}Sb on T sites. Note that the [0001] patterns for S_O and T sites are identical and that they differ from the S_{Zn} best fit only with respect to the maximum yield.

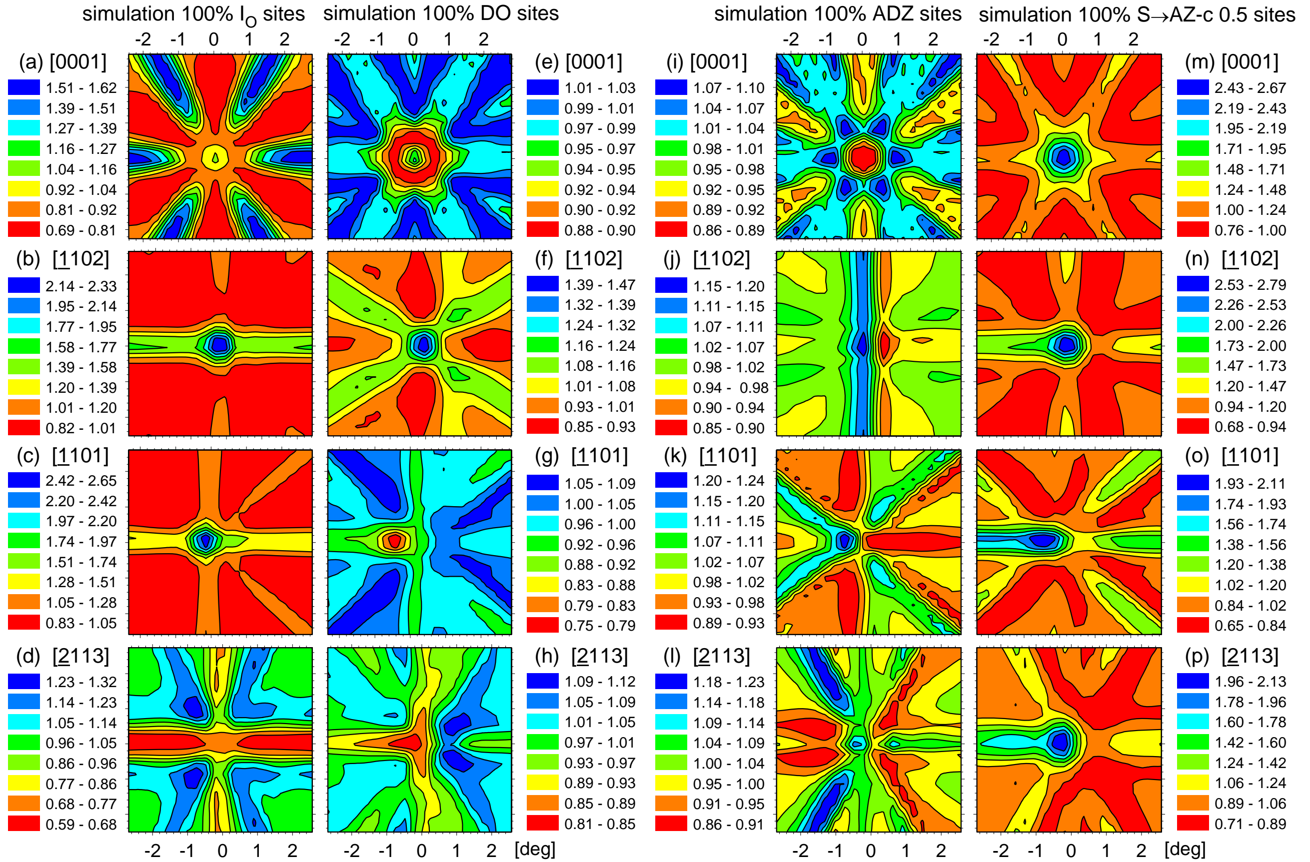

Figure 6. Theoretical emission channeling patterns for 100% of emitter atoms on (a)-(d): interstitial I_O sites, (e)-(h): interstitial DO sites, (e)-(h): interstitial ADZ sites, (e)-(h): interstitial S→AZ-c 0.5 sites, i.e. halfway between S_{Zn} and AZ-c. The locations of these four sites are indicated in Fig. 3. Note that halfway between S_{Zn} and AZ-c (indicated by filled yellow circles in Fig. 3) is the approximate position of As within electrically active As_{Zn}–$2V_{Zn}$ complexes predicted by Ref. 44.

3.3 Lattice location of implanted ^{33}P

As has been pointed out already above, the lattice location experiment with ^{33}P suffered from the fact that the implantation of $^{33}P^+$ was accompanied by a 200 times more intense unknown contaminant with the same charge over mass ratio. This had the following two consequences. First of all the electron count rate from this sample was much lower than for the other two samples, which made it impossible to do measurements with good statistics for a whole set of annealing steps. In addition, the relatively high implanted fluence caused radiation damage to the sample, which is most likely responsible for the rather small anisotropies seen in the ^{33}P patterns. The combination of relatively poor statistics and weak anisotropy means that the the fits of the emission channeling patterns are associated with larger error bars than in the cases of ^{73}As and ^{124}Sb presented above.

Despite these limitations the recorded patterns, shown in Fig 7 (a)-(d) following annealing at 600°C, give clear evidence that P prefers to occupy substitutional Zn sites. Best fits [Fig 7 (e)-(h)] were obtained for 68% of ^{33}P aligned with the *c*-axis, and 40%, 39% and 40% at substitutional S_{Zn} sites. The root mean square (rms) displacements perpendicular to the corresponding channeling directions, $u_1(^{33}P)$, which gave the best fits were 0.13 Å, 0.07 Å, 0.09 Å, and 0.06 Å. Due to the relatively large error bar of the ^{33}P data, the three-site fits with S_{Zn}, S_O and T site fractions for this isotope often resulted in relatively high negative fractions for emitter atoms on T sites, and hence these fit results could not be

considered relevant. Correspondingly only two-site fits for fractions of ^{33}P on S_{Zn} and S_O sites are presented, the results of which are shown in Fig. 8 (c).

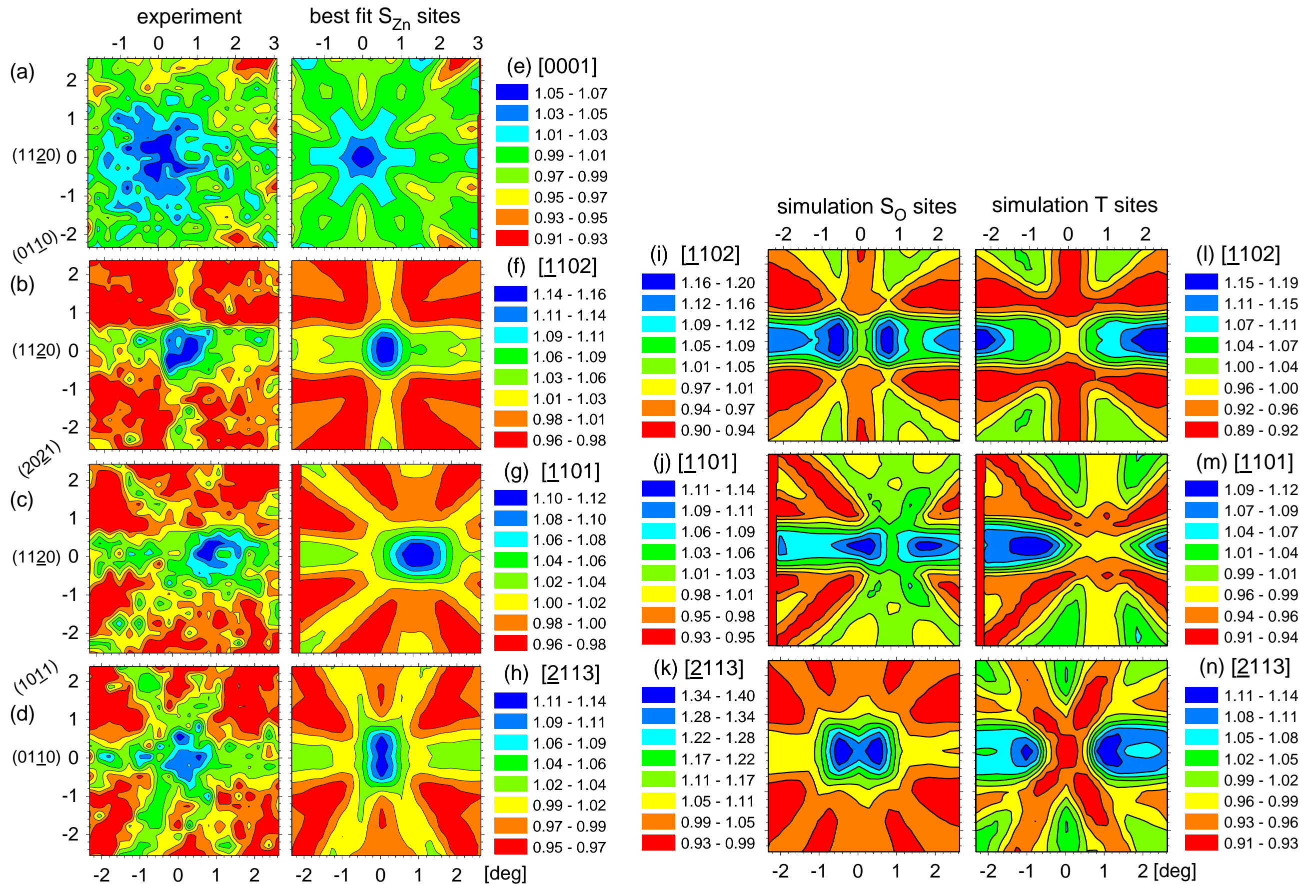

Figure 7. Normalized angular distribution of β^{-} yields from ^{33}P in ZnO following annealing at 600°C around the (a) [0001], (b) [−1102], (c) [−1101] and (d) [−2113] axis. (e)-(h): Best fits of the channeling patterns corresponding to 68% of ^{33}P aligned with the c-axis, and 40%, 39% and 40% at substitutional S_{Zn} sites, respectively. (i)-(k): Theoretical emission channeling patterns for 100% of emitter atoms on S_O sites. (l)-(n): Theoretical emission channeling patterns for 100% of ^{33}P on T sites. Note that the [0001] patterns for S_O and T sites are not shown since they are identical to the pattern for S_{Zn} sites.

4. DISCUSSION

4.1 Comparison of the lattice location of P, As and Sb as a function of annealing temperature

As can be seen from the compilation of data in Fig. (8), for all the group V impurities investigated the largest fraction on regular lattice sites occupies substitutional Zn sites. On the other hand, the fitted fractions on S_O sites are at maximum 5-6%. However, such small fractions are at the detection limit of the emission channeling technique, which is illustrated by the fact that the fitted fractions of ^{73}As and ^{124}Sb on S_O sites become a few percent negative following T_A=900°C. This is of course not physically possible but the result of statistical uncertainty in the fitting procedure. It is hence doubtful whether any ^{33}P, ^{73}As or ^{124}Sb emitter atoms actually occupy the S_O or T sites if the corresponding fractions are not

clearly above ~10%. The rms displacements for As on S_{Zn} sites as derived from the best fit results, are on average somewhat larger but close to those reported in the literature for Zn atoms at room temperature, u_1(Zn)=0.078–0.097 Å[59-61]. The rms displacements $u_1(^{73}As)$ and $u_1(^{33}P)$ tend to show greater scatter but in all three cases the impurity rms displacements from the ideal S_{Zn} sites are within a factor of two of the Zn rms displacements.

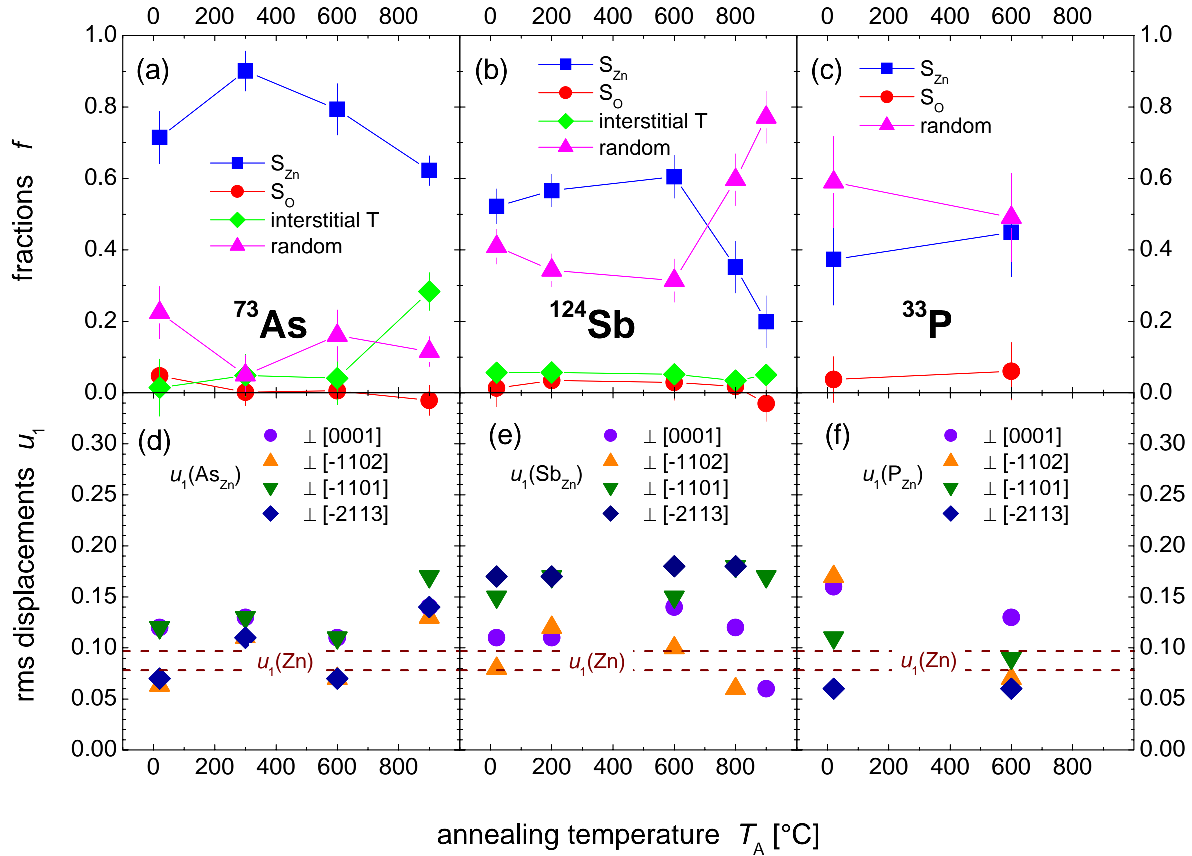

Figure 8. Fractions of ^{73}As (a) and ^{124}Sb (b) on substitutional Zn (S_{Zn}), substitutional O (S_O), interstitial T, and random sites as obtained from three-site fits as a function of annealing temperature. and ^{33}P (c) The best fit values for the rms displacements of the ^{73}As (d), ^{124}Sb (e) and ^{33}P (f) emitter atoms from ideal S_{Zn} sites, perpendicular to the four measured crystallographic directions, and derived from the same type of fitting procedure. The two dashed lines in panels (d-f) indicate the range of room temperature rms displacement values of Zn atoms reported in the literature.

4.2 Relevance of current results with respect to the acceptor model of As in ZnO

Unfortunately our experiments cannot settle the interesting issue whether substitutional P, As and Sb on oxygen sites ("chemical acceptor model"), as is often assumed[10,11,26,29,48], or P_{Zn}–$2V_{Zn}$, As_{Zn}–$2V_{Zn}$, and Sb_{Zn}–$2V_{Zn}$ complexes ("complex acceptor model")[12,44-47] are responsible for the acceptor action. The fact that implanted P, As and Sb prefer the substitutional Zn sites is clearly a strong argument in favor of the complex acceptor model. However, since the channeling effect is not suitable to characterize the immediate neighbourhood of the probe atoms and we hence cannot probe whether the substitutitional P_{Zn}, As_{Zn} and Sb_{Zn} are paired with one or more vacancies, we cannot fully confirm the structural As_{Zn}–$2V_{Zn}$ model. The Zn site character of P, As and Sb can be understood from the large size-mismatch of

P^{3-}, As^{3-} and Sb^{3-} with O^{2-} but the good match between P^{3+}, As^{3+} and Sb^{3+} and Zn^{2+} (0.44 Å, 0.58 Å, and 0.74 Å *vs* 0.60 Å). If these oxidation states were assumed, the overwhelming majority of P, As and Sb would most likely act as double acceptors in implanted samples, unless they would capture two Zn vacancies and be transformed into acceptor complexes. Within these complexes they would be subject to lattice relaxations[12,44-47]. For instance, two structures were proposed for the $As_{Zn}–2V_{Zn}$ complexes[44]. If the complex is triply negatively charged, As should be 4-fold O-coordinated and remain relatively close to the ideal Zn lattice position. Though, this position was considered to be thermally unstable. On the other hand, in a neutral or negatively charged complex (the un-ionized and ionized acceptor, respectively) As should be 5-fold O-coordinated and relax along the *c* axis, around 0.4–0.5 Å or halfway from the ideal Zn position towards the anti-bonding Zn site (cf. Fig. 3). However, what we find is that the rms displacements of the probe atoms from the ideal substitutional Zn sites are relatively small, thus excluding the possibility of large lattice relaxations other than breathing mode relaxations. In the case of ^{73}As, our results also showed that following vacuum annealing at 900°C a significant fraction of ^{73}As probe atoms (almost 30%) was found within 0.4 Å from interstitial T sites. It is known that annealing ZnO above 500°C under O-poor conditions can result in O loss and thus change the stoichiometry in the near-surface region[1]. Given the relatively shallow depth profile of the implanted As, part of the implanted probe atoms may therefore have reacted for instance with O vacancies upon annealing at 900°C, forming a complex. However, this complex is probably also not the $As_{Zn}–2V_{Zn}$ proposed by Limpijumnong et al[44-45], for which they predicted an As position halfway from the ideal Zn position towards the antibonding Zn site (AZ-c in Fig. 3), i.e. ~0.4–0.5 Å from S_{Zn}. Our oxygen-poor annealing conditions should not favor its formation and in addition we found the As within 0.4 Å from interstitial T sites, i.e. ~1.6 Å from S_{Zn}.

On the other hand, while we have proven that the majority of P, As and Sb prefer occupying Zn sites, which is certainly not an encouraging perspective for these heavy group V elements a chemical dopants, we do not have any information with respect to their electrical activity in our samples. This issue is of particular relevance, since it has for instance been reported that not more than 5-13% of incorporated As can be electrically activated in ZnO[13,15,16]. The maximum concentration of As in our implanted sample ($\approx 8\times10^{18}$ atoms cm^{-3}) is comparable with the As concentration used in most other studies. Although we are sure that in our case less than 5% of the implanted As and Sb occupied O sites, it cannot be excluded that by means of using different doping techniques, e.g. doping during MBE growth, around 10% of the group V impurities might be incorporated on O sites and thus be responsible for the *p*-type conductivity reported in the literature.

Furthermore, chemical similarity certainly also plays a role in determining impurity lattice sites. For instance, the electronegativity of P, As and Sb is 2.1, 2.0, and 1.9, which is closer to Zn (1.6) than to O (3.5), illustrating the metallic and semi-metallic character of Sb and As, respectively. We have also carried out lattice location experiments of ^{73}As in GaN[51,65] and found that As acted as an amphoteric impurity, i.e. it occupied both Ga and N sites roughly at a ratio 50:50. In GaN, whereas the ionic radii of As^{3+} and Ga^{3+} are also well-matched (0.58 Å *vs* 0.62 Å), the anion size-mismatch between As^{3-} and N^{3-} (2.22 Å *vs* 1.71 Å) is considerably smaller than in ZnO. The 1.0 difference between the electronegativities of As (2.0) and N (3.0) is also smaller than the difference of 1.5 difference between As and O but still larger than the 0.4 difference between As (2.0) and Ga (1.6). However, despite of these simple considerations, which would also suggest that As replaces the Ga cations, apparently the chemical similarity between As and N is strong enough in order to allow for roughly half of it to be incorporated on N sites. The amphoteric character found for As in GaN therefore provides an argument in favour of the possibility of the existence of minority As_O acceptors in ZnO, since obviously the size-mismatch on anion sites, which is less pronounced in GaN but still present, is not able to completely prevent As from occupying anion positions in GaN. We may therefore conclude that the question of the nature of the P, As and Sb acceptors in ZnO is certainly still open for discussion.

5. CONCLUSION

We find, in contrast to what one might expect from their nature as group V elements, that P, As and Sb do *not* occupy substitutional S_O sites in ZnO but mostly substitutional S_{Zn} sites. Possible fractions of P, As or Sb on O sites in our experiments, if existing at all, could at maximum have been a few percent. The heavy group V elements in ZnO are thus interesting examples for impurities where the *major* impurity lattice site is determined by ionic size rather than their position in the periodic system. While our results cannot settle the interesting issue whether substitutional P, As or Sb on oxygen sites or $P_{Zn}–2V_{Zn}$, $As_{Zn}–2V_{Zn}$ or $Sb_{Zn}–2V_{Zn}$ complexes are responsible for the acceptor action, the fact that

implanted P, As and Sb prefer the substitutional S_{Zn} sites is clearly a strong argument in favour of the complex acceptor model, while it discourages the notion that P, As and Sb may act as efficient "chemical" acceptors in ZnO.

ACKNOWLEDGMENTS

We acknowledge the beam time provided by the ISOLDE collaboration and funding by the Portuguese Foundation for Science and Technology (FCT, projects PTDC/FIS/66262/2006 and CERN/FP/83506/2008) and the European Union Sixth Framework (RII3-EURONS contract 506065). T.M. acknowledges her PhD student fellowship by FCT and S.D. acknowledges financial support from FWO Flanders.

REFERENCES

[1] Pearton, S. J., Norton, D. P., Ip, K., Heo, Y. W. and Steiner, T., "Recent advances in processing of ZnO", J. Vac. Sci. Tech. B **22**, 932-948 (2004).
[2] Look, D. C., "Electrical and optical properties of *p*-type ZnO", Semicond. Sci. Technol. 20, S55-S61 (2005).
[3] Pearton, S. J., Norton, D. P., Ip, K., Heo, Y. W. and Steiner, T., "Recent progress in processing and properties of ZnO", Prog. Mater. Sci. 50, 293-340 (2005).
[4] Özgür, Ü., Alivov, Y. I., Liu, C., Teke, A., Reshchikov, M. A., Doğan, S., Avrutin, V., Cho, S. J. and Morkoç, H., "A comprehensive review of ZnO materials and devices", J. Appl. Phys. 98, 041301/1-103 (2005).
[5] Janotti, A. and Van de Walle, C. G., "Fundamentals of zinc oxide as a semiconductor", Rep. Prog. Phys. 72, 126501/1-29 (2009).
[6] Xiu, F. X., Mandalapu, L. J., Yang, Z., Liu, J. L., Liu, G. F. and Yarmoff, J. A., "Bi-induced acceptor states in ZnO by molecular-beam epitaxy", Appl. Phys. Lett. 89, 052103/1-3 (2006).
[7] Ryu, Y. R., Zhu, S., Look, D. C., Wrobel, J. M., Jeong, H. M. and White, H. W., "Synthesis of *p*-type ZnO films", J. Cryst. Growth 216, 330-334 (2000).
[8] Aoki, T., Hatanaka, Y. and Look, D. C., "ZnO diode fabricated by excimer-laser doping", Appl. Phys. Lett. 76, 3257-3259 (2000).
[9] Vaithianathan, V., Lee, B. and S. S. Kim, "Preparation of As-doped *p*-type ZnO films using a Zn_3As_2 /ZnO target with pulsed laser deposition", Appl. Phys. Lett. 86, 062101/1-3 (2005).
[10] Vaithianathan, V., Lee, B. T., Chang, C. H., Asokan, K. and Kim, S. S., "Characterization of As-doped, *p*-type ZnO by x-ray absorption near-edge structure spectroscopy", Appl. Phys. Lett. 88, 112103/1-3 (2006).
[11] Vaithianathan, V., Kim, S. S. and Asokan, K., "Comment on 'Characterization of As-doped, *p*-type ZnO by x-ray absorption near-edge structure spectroscopy: Theory' ", Appl. Phys. Lett. 92, 236101/1 (2008).
[12] Shen, Y., Mi, L., Xu, X., Wu, J., Wang, P., Ying, Z. and Xu, N., "Studies of the mechanism of electrical conduction in As-doped ZnO by structural and chemical-bonding analyses and first principle calculations", Solid State Comm. 148, 301-304 (2008).
[13] Ryu, Y. R., Lee, T. S. and White, H. W., "Properties of arsenic-doped *p*-type ZnO grown by hybrid beam deposition", Appl. Phys. Lett. 83, 87-89 (2003).
[14] Ryu, Y., Lee, T. S., Lubguban, J. A., White, H. W., Kim, B. J., Park, Y. S., Youn, C. J., "Next generation of oxide photonic devices: ZnO-based ultraviolet light emitting diodes", Appl. Phys. Lett. 88, 241108/1-3 (2006).
[15] Look, D. C., Renlund, G. M., Burgener, R. H. and Sizelove, J. R., "As-doped *p*-type ZnO produced by an evaporation/sputtering process", Appl. Phys. Lett. 85, 5269-5271 (2004).
[16] Braunstein, G., Muraviev, A., Saxena, H., Dhere, N., Richter, V. and Kalish, R., "*p* type doping of zinc oxide by arsenic ion implantation", Appl. Phys. Lett. 87, 192103/1-3 (2005).
[17] Yang, Y., Sun, X. W., Tay, B. K., You, G. F., Tan, S. T. and Teo, K. L., "A *p-n* homojunction ZnO nanorod light-emitting diode formed by As ion implantation", Appl. Phys. Lett. 93, 253107/1-3 (2008).
[18] Kang, H. S., Kim, G. H., Kim, D. L., Chang, H. W., Ahn, B. D. and Lee, S. Y., "Investigation on the *p*-type formation mechanism of arsenic doped *p*-type ZnO thin film", Appl. Phys. Lett. 89, 181103/1-3 (2006).
[19] Du, G., Cui, Y., Xiaochuan, X., Li, X., Zhu, H., Zhang, B., Zhang, Y. and Ma, Y., "Visual-infrared electroluminescence emission from ZnO/GaAs heterojunctions grown by metal-organic chemical vapor deposition", Appl. Phys. Lett. 90, 243504/1-3 (2007).

[20] Bang, K. H., Hwang, D. K., Park, M. C., Ko, Y. D., Yun, I. and Myoung, J.M., "Formation of *p*-type ZnO film on InP substrate by phosphor doping", Appl. Surf. Sci. 210, 177–182 (2003).
[21] Jang, S., Chen, J. J., Kang, B. S., Ren, F., Norton, D. P., Pearton, S. J., Lopata J. and Hobson, W. S., "Formation of *p-n* homojunctions in *n*-ZnO bulk single crystals by diffusion from a Zn_3P_2 source", Appl. Phys. Lett. 87, 222113/1-3 (2005).
[22] Kim, K. K., Kim, H. S., Hwang, D. K., Lim, J. H. and Park, S. J., "Realization of *p*-type ZnO thin films via phosphorus doping and thermal activation of the dopant", Appl. Phys. Lett. 83, 63-65 (2003).
[23] Hwang, D. K., Kim, H. S., Lim, J. H., Oh, J. Y., Yang, J. H., Park, S. J., Kim, K. K., Look, D.C. and Park, Y. S., "Study of the photoluminescence of phosphorus-doped *p*-type ZnO thin films grown by radio-frequency magnetron sputtering", Appl. Phys. Lett. 86, 151917/1-3 (2005).
[24] Yu, Z. G., Wu, P. and Gong, H., "Control of *p*- and *n*-type conductivities in P doped ZnO thin films by using radio-frequency sputtering", Appl. Phys. Lett. 88, 132114/1-3 (2006).
[25] Wang, P., Chen, N. F. and Yin, Z. G., "P-doped *p*-type ZnO films deposited on Si substrate by radio-frequency magnetron sputtering", Appl. Phys. Lett. 88, 152102/1-3 (2006).
[26] Oh, M. S., Hwang, D. K., Choi, Y. S., Kang, J. W., Park, S. J., Hwang, C. S. and Cho, K. I., "Microstructural properties of phosphorus-doped *p*-type ZnO grown by radio-frequency magnetron sputtering", Appl. Phys. Lett. 93, 111905/1-3 (2008).
[27] Xiu, F. X., Yang, Z., Mandalapu, L. J., Liu, J. L. and Beyermann, W. P., "*p*-type ZnO films with solid-source phosphorus doping by molecular-beam epitaxy", Appl. Phys. Lett. 88 , 052106/1-3 (2006).
[28] Pan, X. H., Jiang, J., Zeng, Y. J., He, H. P., Zhu, L. P., Ye, Z. Z., Zhao, B. H. and Pan, X. Q., "Electrical and optical properties of phosphorus-doped *p*-type ZnO films grown by metalorganic chemical vapor deposition", J. Appl. Phys. 103, 023708/1-4 (2008).
[29] Vaithianathan, V., Asokan, K., Park, J. Y. and Kim, S. S., "Local electronic structure of phosphorus-doped ZnO films investigated by X-ray absorption near-edge spectroscopy", Appl. Phys. A 94, 995-998 (2009).
[30] Mandalapu, L. J., Yang, Z., Xiu, F. X., Zhao, D. T. and Liu, J. L., "Homojunction photodiodes based on Sb-doped *p*-type ZnO for ultraviolet detection", Appl. Phys. Lett. 88, 092103/1-3 (2006).
[31] Mandalapu, L. J., Yang, Z., Xiu, F. X., Zhao, D. T. and Liu, J. L., "*p*-type behavior from Sb-doped ZnO heterojunction photodiodes", Appl. Phys. Lett. 88, 112108/1-3 (2006).
[32] Mandalapu, L. J., Yang, Z., Chu, S. and Liu, J. L., "Ultraviolet emission from Sb-doped *p*-type ZnO based heterojunction light-emitting diodes", Appl. Phys. Lett. 92, 122101/1-3 (2008).
[33] Chu, S., Lim, J. H., Mandalapu, L. J., Yang, Z., Li, L. and Liu, J. L., "Sb-doped *p*-ZnO/Ga-doped *n*-ZnO homojunction ultraviolet light emitting diodes", Appl. Phys. Lett. 92, 152103/1-3 (2008).
[34] Kong, J., Chu, S., Olmedo, M., Li, L., Yang, Z. and Liu, J., "Dominant ultraviolet light emissions in packed ZnO columnar homojunction diodes", Appl. Phys. Lett. 93, 132113/1-3 (2008).
[35] Chu, S., Olmedo, M., Yang, Z., Kong, J. and Liu, J., "Electrically pumped ultraviolet ZnO diode lasers on Si", Appl. Phys. Lett. 93, 181106/1-3 (2008).
[36] Zhao, J. Z., Liang, H. W., Sun, J. C., Bian, J. M., Feng, Q. J., Hu, L. Z., Zhang, H. Q., Liang, X. P., Luo, Y. M. and Du, G. T., "Electroluminescence from *n*-ZnO/*p*-ZnO:Sb homojunction light emitting diode on sapphire substrate with metal-organic precursors doped *p*-type ZnO layer grown by MOCVD technology", J. Phys. D: Appl. Phys. 41, 195110/1-4 (2008).
[37] Aoki, T., Shimizu, Y., Miyake, A., Nakamura, A., Nakanishi, Y. and Hatanaka, Y., "*p*-Type ZnO layer formation by excimer laser doping", phys. stat. solidi (b) 229, 911-914 (2002).
[38] Xiu, F. X., Yang, Z., Mandalapu, L. J., Zhao, D. T., Liu, J. L. and Beyermann, W. P., "High-mobility Sb-doped *p*-type ZnO by molecular-beam epitaxy", Appl. Phys. Lett. 87, 152101/1-3 (2005).
[39] Lopatiuk-Tirpak, O., Schoenfeld, W. V., Chernyak, L., Xiu, F. X., Liu, J. L., Jang, S., Ren, F., Pearton, S. J., Osinsky, A. and Chow, P., "Carrier concentration dependence of acceptor activation energy in *p*-type Zn O", Appl. Phys. Lett. 88, 202110/1-3 (2006).
[40] Lopatiuk-Tirpak, O., Chernyak, L., Xiu, F. X., Liu, J. L., Jang, S., Ren, F., Pearton, S. J., Gartsman, K., Feldmann, Y., Osinsky, A. and Chow, P., "Studies of minority carrier diffusion length increase in *p*-type ZnO:Sb", J. Appl. Phys. 100, 086101/1-3 (2006).
[41] Pan, X., Ye, Z., Li, J., Gu, X., Zeng, Y., He, H., Zhu, L. and Che, Y., "Fabrication of Sb-doped *p*-type ZnO thin films by pulsed laser deposition", Appl. Surf. Sci. 253, 5067-5069 (2007).
[42] Przeździecka, E., Kamińska, E., Pasternak, I., Piotrowska, A. and Kossut, J., "Photoluminescence study of *p*-type ZnO:Sb prepared by thermal oxidation of the Zn-Sb starting material", Phys. Rev. B 76, 193303/1-4 (2007).

[43] Park, C. H., Zhang, S. B. and Wei, S. H., "Origin of *p*-type doping difficulty in ZnO: The impurity perspective", Phys. Rev. B 66, 073202/1-3 (2002).
[44] Limpijumnong, S., Zhang, S. B., Wei, S. H. and Park, C. H., "Doping by large-size-mismatched impurities: the microscopic origin of arsenic or antimony-doped *p*-type zinc oxide", Phys. Rev. Lett. 92, 155504/1-4 (2004).
[45] Limpijumnong, S., Smith, M. F. and Zhang, S. B., "Characterization of As-doped, *p*-type ZnO by x-ray absorption near-edge structure spectroscopy: Theory", Appl. Phys. Lett. 89, 222113/1-3 (2006).
[46] Lee, W. J., Kang, J. and Chang, K. J., "Defect properties and *p*-type doping efficiency in phosphorus-doped ZnO", Phys. Rev. B 73, 024117/1-6 (2006).
[47] Limpijumnong, S., Smith, M. F. and Zhang, S. B., "Response to 'Comment on 'Characterization of As-doped, *p*-type ZnO by x-ray absorption near-edge structure spectroscopy: Theory' ", Appl. Phys. Lett. 92, 236102/1-2 (2008).
[48] Zhang, F. C., Zhang, Z. Y., Zhang, W. H., Yan, J. F. and Yun, J. N., "First-Principles Calculation of Electronic Structure and Optical Properties of Sb-Doped ZnO", Chin. Phys. Lett. 25, 3735-3738 (2008).
[49] Wahl, U., Rita, E., Correia, J. G., Marques, A. C., Alves, E., Soares, J. C. and the ISOLDE collaboration, "Direct Evidence for As as a Zn-Site Impurity in ZnO", Phys. Rev. Lett. 95, 215503/1-4 (2005).
[50] Wahl, U., Rita, E., Correia, J.G., Marques, A.C., Alves, E., Soares, J.C. and the ISOLDE collaboration, "Lattice location of implanted As in ZnO", Superlatt. Microstruct. 42, 8-13 (2007).
[51] Wahl, U., Correia, J. G., Rita, E., Marques, A. C., Alves, E., Soares, J. C. and the ISOLDE collaboration, "Arsenic in ZnO and GaN: Substitutional cation or anion sites?", Mater. Res. Soc. Symp. Proc. 994, F01-03/1-13 (2007).
[52] Wahl, U., Correia, J. G., Mendonça, T. and Decoster, S., "Lattice location of the group V elements As and Sb in ZnO", Physica B 404, 4803-4806 (2009).
[53] Wahl, U., Correia, J. G., Mendonça, T. and Decoster, S., "Direct evidence for Sb as a Zn site impurity in ZnO", Appl. Phys. Lett. 94, 261901/1-3 (2009).
[54] Hofsäss H. and Lindner, G., "Emission channeling and blocking", Phys. Rep. 201, 121-183 (1991).
[55] Catherall, R., Fedosseev, V. N., Köster, U., Lettry, J., Suberlucq, G., the ISOLDE collaboration,. Marsh, B. A and Tengborn, E., "Recent developments in production of radioactive ion beams with the selective laser ion source at the on-line isotope separator ISOLDE", Rev. Sci. Instr. **75**, 1614-1616 (2004).
[56] Wahl, U., Correia, J. G., Czermak, A., Jahn, S. G., Jalocha, P., Marques, J. G., Rudge, A., Schopper, F., Soares, J. C., Vantomme, A., Weilhammer, P. and the ISOLDE collaboration, "Position-sensitive Si pad detectors for electron emission channeling experiments", Nucl. Instr. Meth. A 524, 245-256 (2004).
[57] Marques, A. C., Wahl, U., Correia, J. G., Silva, M. R., Rudge, A., Weilhammer, P., Soares, J. C. and the ISOLDE collaboration, "Noise and trigger efficiency characterization of cooled silicon pad detectors", Nucl. Instr. Meth. A **572**, 1056-1064 (2007).
[58] Rössler, U., [Landolt-Börnstein New Series, Vol. 22, ed. by O. Madelung], Springer, Berlin, 163 (1989).
[59] Schulz, H. and Thiemann, K. H., "Structure parameters and polarity of the wurtzite type compounds SiC-2H and ZnO", Solid State Comm. 32, 783-785 (1979).
[60] Albertsson, J. and Abrahams, S. C., "Atomic displacement, anharmonic thermal vibration, expansivity and pyroelectric coefficient thermal dependences in ZnO", Acta Cryst. B 45, 34-40 (1989).
[61] Yoshiasa, A., Koto, K., Maeda, H. and Ishii, T., "The mean square relative displacement and displacement correlation functions in tetrahedrally and octahedrally coordinated $A^{N}B^{8-N}$ crystals", Jpn. J. Appl. Phys. 36, 781-784 (1997).
[62] Wahl, U., Rita, E., Correia, J. G., Alves, E., Araújo, J. P. and the ISOLDE Collaboration, "Implantation site of rare earths in single-crystalline ZnO", Appl. Phys. Lett. 82, 1173-1175 (2003).
[63] Wahl, U., Rita, E., Correia, J. G., Alves, E., Soares, J.C. and the ISOLDE collaboration, "Lattice location and stability of implanted Cu in ZnO", Phys. Rev. B 69, 012102/1-4 (2004).
[64] Agostinelli S., et al., "GEANT4 – a simulation toolkit", Nucl. Instrum. Meth. A 506, 250-303 (2003).
[65] Wahl, U., Correia, J. G., Araújo, J. P., Rita, E., Soares, J. C. and The ISOLDE collaboration, "Amphoteric arsenic in GaN", Appl. Phys. Lett. 90, 181934/1-3 (2007).